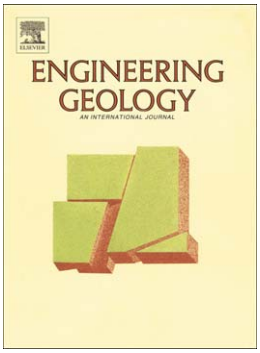

Predicting water permeability in sedimentary rocks from capillary imbibition and pore structure

D. Benavente, C. Pla, N. Cueto, S. Galvañ, J. Martínez-Martínez, M.A. García-del-Cura, S. Ordóñez

PII: S0013-7952(15)00198-2
DOI: doi: 10.1016/j.enggeo.2015.06.003
Reference: ENGEO 4072

To appear in: *Engineering Geology*

Received date: 30 June 2014
Revised date: 3 May 2015
Accepted date: 11 June 2015

Please cite this article as: Benavente, D., Pla, C., Cueto, N., Galvañ, S., Martínez-Martínez, J., García-del-Cura, M.A., Ordóñez, S., Predicting water permeability in sedimentary rocks from capillary imbibition and pore structure, *Engineering Geology* (2015), doi: 10.1016/j.enggeo.2015.06.003

Predicting water permeability in sedimentary rocks from capillary imbibition and pore structure

D. Benavente[(1,2,*)], C. Pla[(1,2)], N. Cueto[(1,2)], S. Galvañ[(2)], J. Martínez-Martínez[(1,2)], M.A. García-del-Cura[(2,3)], S. Ordóñez[(1,2)]

[(1)] Departamento de Ciencias de la Tierra y del Medio Ambiente, Universidad de Alicante, Ap. 99.03080 Alicante, Spain.

[(2)] Laboratorio de Petrología Aplicada, Unidad Asociada UA-CSIC, Universidad de Alicante, Ap. 99.03080 Alicante, Spain.

[(3)] Instituto de Geociencias, CSIC-UCM, Madrid, Spain.

**Corresponding Author:*

David Benavente

email: david.benavente@ua.es

+0034 96 590 3727

Abstract

In this paper, absolute water permeability is estimated from capillary imbibition and pore structure for 15 sedimentary rock types. They present a wide range of petrographic characteristics that provide degrees of connectivity, porosities, pore size distributions, water absorption coefficients by capillarity and water permeabilities. A statistical analysis shows strong correlations among the petrophysical parameters of the studied rocks. Several fundamental properties are fitted into different linear and multiple expressions where water permeability is expressed as a generalized function of the properties. Some practical aspects of these correlations are highlighted in order to use capillary imbibition tests to estimate permeability. The permeability-porosity relation is discussed in the context of the influence of pore connectivity and wettability. As a consequence, we propose a generalized model for permeability that includes information about water fluid rate (water absorption coefficient by capillarity), water properties (density and viscosity), wetting (interfacial tension and contact angle) and pore structure (pore radius and porosity). Its application is examined in terms of the type of pores that contribute to water transport and wettability. The results indicate that the threshold pore radius, in which water percolates through rock, achieves the best description of the pore system. The proposed equation is compared against Carman-Kozeny's and Katz-Thompson's equations. The proposed equation achieves very accurate predictions of the water permeability in the range of 0.01 to 1000 mD.

Highlights

-Permeability expressions are obtained using open porosity and capillary coefficients.

-The permeability – porosity relationship shows two zones defined by a porosity of 10%.

-A generalized model for predicting intrinsic permeability is proposed.

-The analysis of wetting reveals incomplete water wetting in the studied rocks.

Key words:

Absolute permeability, permeability prediction, spontaneous imbibition, capillary absorption, fluid transport properties, wettability.

1. Introduction

Water transport in porous rocks has been widely studied in several fields of research and technological applications, such as engineering geology, soil physics, building materials, ground water, geothermal reservoir engineering, secondary and enhanced oil recovery (EOR), and unconventional hydrocarbon resource assessment for further production, among others. Water transport can be carried out in different ways depending on the water saturation of the rocks. We can distinguish between saturated water flow, which is described by the permeability, and unsaturated water flow, which can be defined through the capillary flow.

Permeability measures a material's ability to transmit fluids into a saturated material under a pressure gradient. It can be referred to in different ways depending upon the field. Thus, depending on the fluid composition, a distinction must be established among intrinsic or absolute permeability (laminar flow of a single nonreactive fluid), effective permeability (flow of one fluid in the presence of another fluid, when the fluids are immiscible), and relative permeability (ratio of effective and absolute permeability) (Schön, 2011). Intrinsic permeability depends only on the pore structure of the material and has units with dimensions of area (m^2, in SI units). In the oil industry, the Darcy (D) or, more commonly, the millidarcy (mD) are typical units. Hydraulic conductivity is usually referred to as permeability or the coefficient of permeability, and it is related to intrinsic permeability (pore structure) and to the properties of the fluid. Hydraulic conductivity has units with dimensions of length per time or speed and is widely used in hydrogeology. Between the two properties, the following conversion can be used (the correct equation implements density and viscosity of water and gravity): 1D $\sim 10^{-12}$ m^2 $\sim 10^{-5}$ m/s (for pure water at 20 ºC). In this paper, we study the water intrinsic permeability, k, which for convenience will be called water permeability, using mD as the measurement units.

Capillary flow is the most common water transport mechanism in soils and rocks when they are in contact with the atmosphere. The spontaneous capillary imbibition is characterized through the water absorption coefficient by capillarity, C, which is referred to as the variation of water weight per unit of the square root of time and sample area, and sample sorptivity, S, which describes the height variation of water in the rock sample. The units of C are $[ML^{-2}T^{-1/2}]$, whereas S presents the units $[LT^{-1/2}]$. Capillarity absorption of a liquid depends on the pore

microstructure (pore radius and porosity) and on the intrinsic properties of the liquid: density, viscosity, wettability and surface tension.

As we previously mentioned, permeability is a fundamental property to be quantified, and it can be directly obtained in the field or in the laboratory. However, permeability measurements may entail some important problems that include obtaining core samples, the experimental time demanded and costly equipment requirements. For that reason, several models and empirical equations have been developed in order to estimate permeability from pore structure parameters of rocks, including connected porosity, pore size, specific surface area or tortuosity. Probably the simplest model for single-phase permeability was proposed by Kozeny (1927) and later modified by Carman (1937). The Carman-Kozeny model, one of the most widely accepted derivations of permeability and its relationship to permeable medium properties, was developed by comparing Darcy's law with the Hagen-Poiseuille's law for steady laminar flow of an incompressible fluid through a bundle of circular capillary tubes (Panda and Lake, 1994). Moreover, Katz and Thompson's model (1986) used percolation theory to develop a relationship between permeability and the critical pore diameter of sedimentary rocks.

Some models predict permeability from other petrophysical properties, such as electrical resistivity (Archie, 1942), ultrasonic wave velocities (Alam et al., 2011), electromagnetic wave velocities (dielectric constants) (Hubbard and Rubin, 2000) or critical and irreducible water saturation (Leverett, 1940; Brooks and Corey, 1964). In many situations, these practical and interesting relations between permeability and petrophysical properties are an indirect estimation rather than a fluid transport parameter. In this case, permeability estimations will be more realistic in terms of fluid-rock interactions.

Various experimental and limited studies have shown that the capillary absorption coefficient is related to the square root of the permeability (Scherer, 2004; Benavente et al., 2007; Cueto et al., 2009; Casteleyn et al., 2010; Hall and Hoff, 2012; Espinosa-Marzal and Scherer, 2013). The theoretical relationships between both transport parameters have been characterized through Hagen-Poiseuille's equation, which can be written as

$$q = \frac{dv}{dt} = \frac{pr^4}{8h}\frac{\Delta P}{L}, \qquad (1)$$

where q is the volumetric flow rate, v is the volumetric uptake, t is the time, r is the tube radius, η is the viscosity of the fluid ($1.003 \cdot 10^{-3}$ Pa·s for water at 20 ºC), ΔP is the pressure drop, and L is the length of the tube.

Principal advantages for predicting permeability from capillarity are provided through consideration of both scientific and technical meaning. Permeability measurements require more sophisticated procedures than the capillary imbibition test, such that the estimation of water permeability from capillary imbibition also presents a practical interest. Until now, however, the majority of the few permeability and capillarity relationships have been developed for homogeneous and porous materials. Consequently, further research into a wider range of rock types is needed in order to corroborate this relationship.

The aim of this paper is to estimate water permeability from capillary imbibition and pore structure for a wide range of sedimentary rock types with different petrographic characteristics. For this purpose, first, a statistical analysis is carried out in order to empirically establish correlations between these parameters. The results are discussed in the context of the influence of pore connectivity and wettability. Second, a generalized model capable of predicting permeability in sedimentary rocks of distinct lithofacies is proposed based on the statistical analysis. The generalized model is compared against other models, and their applications are discussed in terms of the type of rock porosity. Finally, some practical aspects of this study are highlighted in order to use the capillary imbibition test to estimate permeability.

2. Experimental procedure

2.1 Materials

In this study, 15 samples of porous stones have been chosen for their different petrophysical and petrographic characteristics (Figure 1). These stones are used as building materials or are found in the Spanish-built heritage. The tested stones correspond to four groups of sedimentary rocks with different pore types: biocalcarenites (C), sandstones (S), limestones (L) and travertines and carbonate tufas (T).

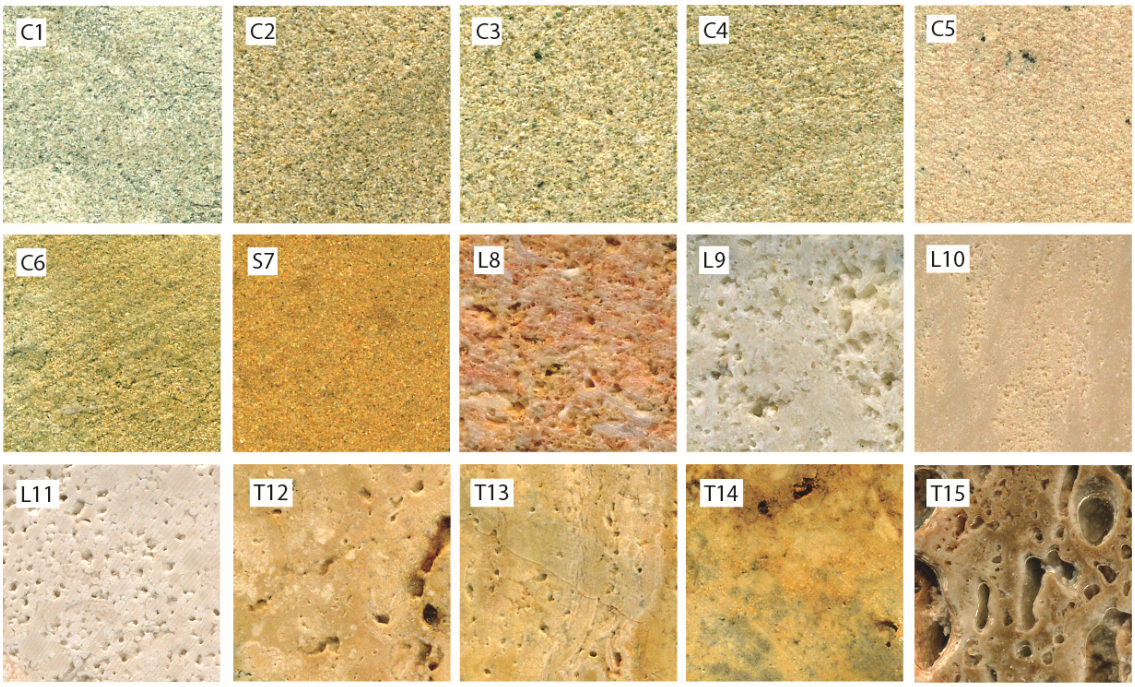

Figure 1. Details of the studied rocks (hand-specimen): C: biocalcarenites; S: sandstones; L: limestones; and T: travertines and tufas. The side length of the image is 2 cm.

2.1.1. Biocalcarenites

The studied biocalcarenites are carbonate sandstones with calcite cement, variable amounts of terrigenous components and fossils (mainly foraminifera) and intergranular porosity. C1, C2, C3 and C4 are well-sorted biocalcarenites that contain foraminifera and quartz, feldspar, mica and dolomite grains (Benavente, 2003; Benavente et al., 2004 and 2008). C5 shows bioclasts larger than the rest of the studied biocalcarenites, and it is constituted by bryozoans, red algae, molluscs and echinoderms. Other detrital components are quartz, dolostones and feldspars (Benavente, 2003). C6 is composed of foraminifera, quartz, feldspars and mica grains (Benavente, 2003).

2.1.2. Sandstone

S7 is a well-sorted sandstone, mainly composed of monocrystalline quartz grains. S7 presents intergranular porosity (Benavente, 2003).

2.1.3. Limestones

The analysed limestones show a wide range of sizes and types of allochems. These limestones mainly have interparticle porosity. L8 and L9 are detrital limestones (biocalcirrudites) composed of large allochem grains (mainly bivalves, bryozoans and red algae) (Benavente, 2003). L10 is a biomicrite composed of oriented fragments of fossils (mainly ostracods and molluscs), which, consequently, provide a structural anisotropy to the rock. L11 is an oolitic limestone (oosparite) where oolites are densely packed and poorly sorted (Martínez-Martínez et al., 2013).

2.1.4. Travertines and tufas

The studied travertines and tufas present different structural (mesofeatures) and textural (microfeatures) characteristics. In this investigation, such meso- and micro-features are described in accordance with García-del-Cura et al. (2012) classification. Thus, T12 presents banded and massive structures with low porosity values (mainly intercrystalline porosity) and some unconnected bugs perpendicular to the banded structure. T13 shows a porous banded structure with fenestral and vug macroporosity, which provides a structural anisotropy. T13 also has intergranular (related to small pisoids) and intercrystalline porosity. T14 presents banded and massive structures with low porosity values (mainly intercrystalline porosity). It shows some separated fenestral and vug macroporosity, so these macropores are interconnected only through intercrystalline porosity. T15 can be classified as homogeneous tufa. It is a very porous limestone with predominant microcrystalline calcite formed over rushes and reeds (accretional microcrystalline fringe cement). T15 shows intercrystalline porosity linked to microcrystalline fringe cements. Macroporosity is also abundant and is formed by plant casts, which have a diameter larger than 0.5 cm.

Lucia's petrophysical classification of porosity in carbonate rocks is applied to the studied sedimentary rocks. This classification was modified after Choquette and Pray's classification (1970) to include pore connectivity. Lucia showed that pore space located between grains (intergranular porosity) and between crystals (intercrystalline porosity) is petrophysically similar, and it is called interparticle porosity. Pore space significantly larger than grains or crystals is vuggy porosity, that is, pore space that is not interparticle. Vuggy porosity is divided into two classes based on the manner in which the vugs are connected. Separated vugs are

interconnected only through interparticle porosity. Touching vugs form an interconnected pore system of significant extension (see details in Lucia (2007)). Thus, biocalcarenites, limestones and sandstones present interparticle (intergranular and intercrystalline) porosity, whereas travertines and tufas have both interparticle and vuggy porosity (see examples of Lucia's classification applied to rocks similar to those studied in this paper in Benavente, 2011; García-del-Cura et al., 2012; and Galvañ et al., 2014). In particular, T13 presents touching-vug porosity, whereas T14 shows separated touching-vug porosity, and T15 displays very large pores and touching-vug porosity.

2.2. Methods

2.2.1. Sample preparation

Two to three cylindrical samples, 3 cm in diameter and 6 cm in height, were cored from each sedimentary rock. Water transport property testing (permeability and capillary imbibition test) and some porous media measurements (bulk density, grain density and connected porosity) were performed on the same core samples. Table 1 shows the mean values and the standard deviations of rock properties obtained considering three measurements of each sample. One core-plug sample, 1.5 cm in diameter and 1.5 cm in length, per each sedimentary rock studied was employed for obtaining pore microstructure data, derived from mercury injection tests. We select core-plug samples without vuggy pores because they cannot be measured using mercury porosimetry. Microstructure characterisation therefore describes interparticle porosity. Vuggy porosity is only presented in cylindrical samples and is estimated by the comparison of open and total porosity.

2.2.2. Porous space characterization

Total porosity, ϕ_T, defined as the ratio of the volume of pore space to the bulk material volume, was calculated using the relationship between bulk and grain densities. Bulk density was determined through direct measurement of dried weights and dimensions of samples. Grain or

real density of a material is defined as the ratio of its mass to its solid volume and was obtained using an AccuPyc 1330 Helium pycnometer. The cylindrical chamber is 46 mm in diameter and 63 mm in height size.

The connected porosity is defined as the ratio of the volume of connected voids to the total rock volume. In this study, for convenience, connected porosity of cylindrical samples and core-plug samples are, respectively, termed as open porosity and effective porosity.

Open porosity, ϕ_O, was obtained using the vacuum water saturation test (UNE-EN 1936:2007). Dried samples were weighed and placed in a vacuum chamber at 20±7 mbar pressure controlled by a vacuum manometer. First, any trapped air was eliminated from the porous systems. Second, distilled water was slowly introduced until the samples were completely covered. Third, atmospheric pressure was re-established in order to avoid porous system dilatation. Then, the saturated and immersed weight of each sample was recorded.

Pore structure was described via the mercury intrusion porosimetry (MIP) technique. An Autopore IV 9500 Micromeritics mercury porosimeter was used, and a surface tension and contact angle of mercury of 480 mN/m and 130º, respectively, were chosen. The pore radius interval ranges from 0.003 to 200 μm, and, consequently, MIP cannot characterise large vug pores. Effective porosity, ϕ_{Hg}, arithmetic mean, r_M, and the critical, r_C, and threshold, r_T, throat-pore radius were obtained (Table 2), and the pore size distribution of each rock was plotted (Fig. 2). A typical cumulative curve for a unimodal pore size distribution is nearly S-shaped. This curve reflects the volume percentage of mercury intruded as a function of the applied pressure. After a gradual increase under rising pressure, a stage of rapid rise is interpreted as the moment when the intruded mercury fills the first connected cluster spanning the sample. The inflection point of the rapidly rising portion of the curve can be seen as the percolation threshold (Katz and Thompson, 1986; El-Dieb and Hooton, 1994; Nokken and Hooton, 2008; Nishiyama and Yokoyama, 2014). The threshold radius is defined as the radius where mercury begins to enter and percolate the pore system in appreciable quantity. The critical, maximum or peak radius is obtained from the maximum of the pore distribution curve. The fractional volume of the pore family with pores larger than r_C is termed $S(r_C)$, whereas $S(r_T)$ is the fractional volume of the pores larger than r_T.

2.2.3. Water flow characterization

Water absorption by capillarity was carried out using a continuous data-recording device due to the high absorption rates of samples. The non-continuous standard method does not permit an accurate calculation of the water absorption coefficient by capillarity, C, for C > 10 $kg/m^2h^{0.5}$ (C > ~150 $g/m^2s^{0.5}$) (Benavente et al., 2007). The results were plotted as the absorbed water per area of the sample throughout imbibition versus the square root of time. Through this type of representation, the capillary imbibition kinetic curve shows two parts or zones. The first zone defines capillary absorption, and the second zone defines the saturation part, where a connected porosity can be estimated regardless of whether the sample is completely water saturated. The slope of the curve during capillary absorption is the water absorption coefficient by capillarity.

Permeability was measured for water-saturated samples. Thus, after open porosity characterisation, vacuum saturated samples were then tested. Permeability tests were carried out in a triaxial device with an automatic pressure system using the steady-state method (see details in Benavente et al., 2007 and Galvañ et al., 2014). The confining, inflow and outflow pressures in the triaxial method were, respectively, 13 bar, 7 bar and 3 bar. Water permeability (intrinsic permeability) was determined according to Darcy's equation (as we will describe in Eq. (7)) when steady-state was reached (water flow rate at the inflow equals the water outflow rate).

In the L10 and T13 samples, permeability and capillary imbibition measurements were carried out in the perpendicular direction to the bedding, whereas, in T14, measurements were performed in the direction parallel to the bedding. These rocks present a heterogeneous pore structure, so a piston-like imbibition process is not described.

2.2.4. Statistical analysis

The statistical analysis of the results, including descriptive statistics, dispersion plots and the stepwise multiple regressions, were carried out using R code (R foundation).

Table 1. Mean values and standard deviations for the open, ϕ_O, and total, ϕ_T, porosities, water absorption coefficient by capillarity, C and water permeability, k_{exp}, of the studied rocks.

Sample	ϕ_O (%)	ϕ_T (%)	C ($kg \cdot m^{-2} \cdot h^{-0.5}$)	k_{exp} (mD)
C1	16.29 ± 0.06	16.24 ± 0.09	0.86 ± 0.02	$4.30 \cdot 10^{-3} \pm 0.29 \cdot 10^{-3}$
C2	20.61 ± 0.08	20.05 ± 0.09	1.25 ± 0.02	0.23 ± 0.02
C3	22.03 ± 0.08	22.26 ± 0.09	2.48 ± 0.02	6.27 ± 0.31
C4	16.70 ± 0.07	16.80 ± 0.09	1.12 ± 0.02	$1.06 \cdot 10^{-2} \pm 0.54 \cdot 10^{-2}$
C5	23.52 ± 0.09	23.66 ± 0.09	3.20 ± 0.02	10.61 ± 0.98
C6	26.72 ± 0.09	27.09 ± 0.09	2.10 ± 0.02	0.84 ± 0.28
S7	13.11 ± 0.06	14.62 ± 0.05	1.68 ± 0.02	2.02 ± 0.51
L8	20.35 ± 0.10	21.84 ± 0.06	6.47 ± 0.03	293 ± 9
L9	19.01 ± 0.10	20.19 ± 0.06	10.94 ± 0.03	1251 ± 27
L10	12.00 ± 0.09	12.35 ± 0.06	1.65 ± 0.02	1.09 ± 0.21
L11	8.62 ± 0.08	8.95 ± 0.06	0.69 ± 0.01	$5.10 \cdot 10^{-2} \pm 0.76 \cdot 10^{-2}$
T12	7.04 ± 0.12	7.20 ± 0.08	0.44 ± 0.01	$1.00 \cdot 10^{-2} \pm 0.50 \cdot 10^{-2}$
T13	12.54 ± 0.09	12.04 ± 0.08	0.47 ± 0.01	$1.00 \cdot 10^{-2} \pm 0.65 \cdot 10^{-2}$
T14	8.46 ± 0.08	18.31 ± 0.08	0.40 ± 0.01	$9.00 \cdot 10^{-2} \pm 0.61 \cdot 10^{-2}$
T15	28.04 ± 0.16	45.95 ± 0.08	3.39 ± 0.02	990.95 ± 10.71

3. Results and discussion

Table 1 shows the mean value of the open and total porosities, water absorption coefficient by capillarity and experimental water permeability, and Table 2 displays the pore structure parameters obtained from mercury porosimetry. The studied porous rocks have a wide range of petrophysical and petrographic characteristics, which are conditioned by rock structure, pore size and pore connectivity of vuggy porosity. In general, porous rocks with larger pores and high porosity values present the highest transport coefficient values.

Hölting's classification (1989) for water permeability classifies stones into four groups: very low, with a k value under 1 mD (~ 10^{-15} m^2 or 10^{-8} m/s); low, with 1 < k < 100 mD; permeable, with

100 < k < 10000 mD; and high, with values of k higher than 10000 mD. A similar grouping can be found in permeability classifications in the hydrocarbon industry (e.g., Lianbo and Yang, 2009). The permeability values of the studied rocks range from 10^{-4} to 10^{4} mD (~ 10^{-19} - 10^{-11} m^2). Therefore, eight varieties of the studied building stones (C1, C2, C4, C6, L11, T12, T13, and T14) are classified as very low-permeability rocks, other four (C3, C5, L10, are S7) are low permeability, and three (L8, L9, T15) are permeable.

Most of the studied rocks have pore sizes within the measurement interval of the mercury intrusion porosimetry (0.003 to 200 μm). However, L8, L9 and T15 present a volume fraction for large pores (r> 200 μm) that this technique cannot measure. This means that the threshold radius is assumed, as it is not within the range of measurement. This fact can be observed in Figure 2 because mercury is quickly intruded for low mercury pressure values, as well as in the difference between effective porosity (measured using MIP) and total porosity (Table 1), as pores below 0.001 are scarce in the studied rocks.

These rocks also present problems for defining the threshold radius and the fractional volume of pores lager than the threshold radius. Table 2 shows the mean, critical and threshold pore radii, where the critical radius presents larger values than the threshold radius.

3.1. Empirical relationships between pore structure, capillary imbibition and water permeability.

The classical permeability–porosity relationships are shown in Figure 3. This type of relationship is widely used in order to estimate permeability from porosity and to understand the influence of vuggy and interparticle porosities (Lucia, 2007). Thus, the permeability of rocks is only related to its porosity when they have similar types of pores and similar pore size. For instance, C3, C5 and S7 present an excellent permeability–porosity relationship and have similar pore sizes and interparticle porosities.

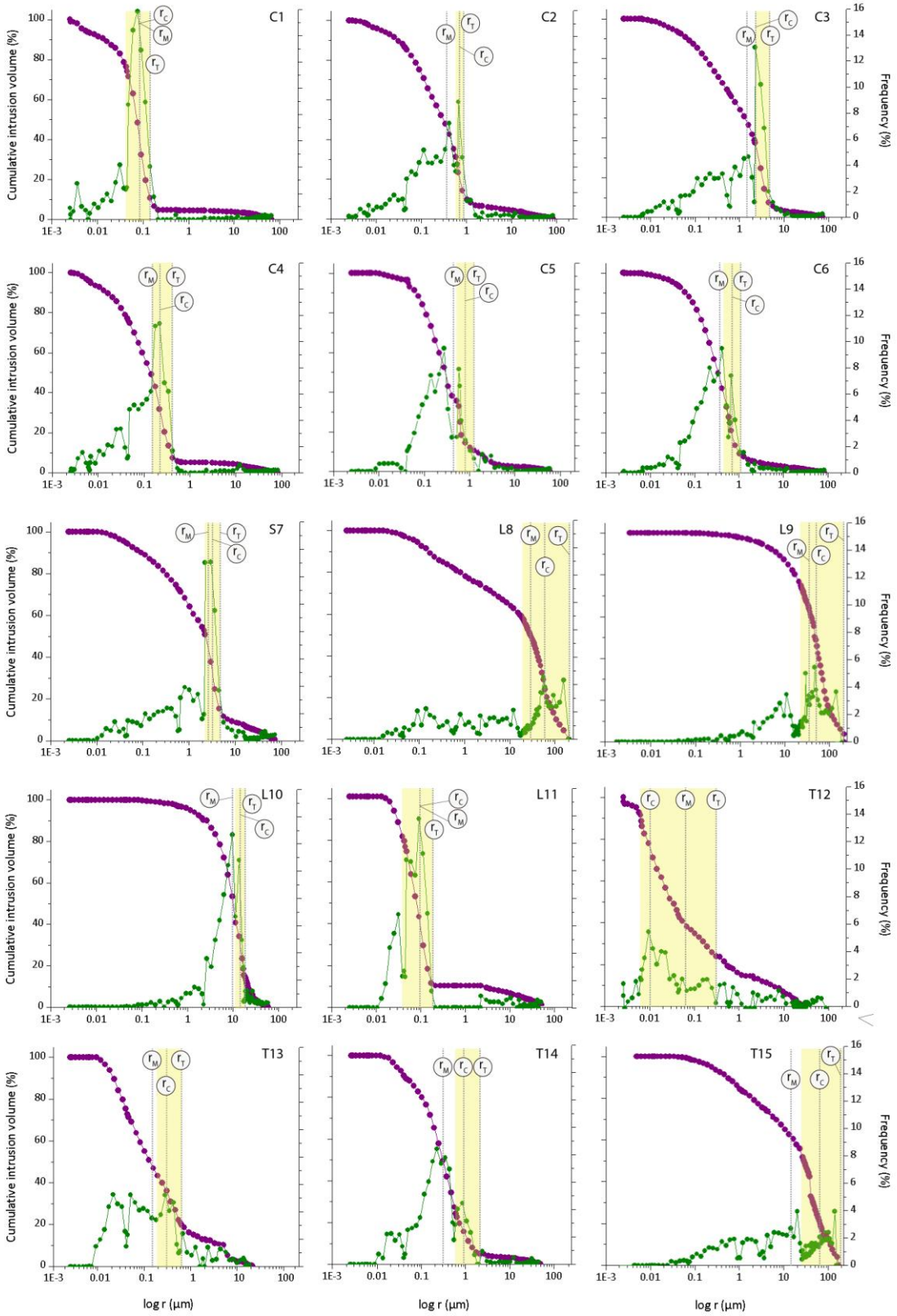

Figure 2. Accumulative mercury intrusion (magenta) and pore size distribution (green) curves of porous rocks. Throat-pore radius: mean, r_M; critical, r_C, and threshold, r_T. The yellow area corresponds to the pore family of the larger pore size.

Table 2. Effective porosity, ϕ_{Hg}; mean r_M, critical, r_C, and threshold, r_T, pore radii; and volume fraction of pores larger than the critical, $S(r_C)$, and threshold, $S(r_T)$, pore radii of the studied rocks. * values are assumed, as they are not within the range of measurement.

Sample	ϕ_{Hg} (%)	r_M (μm)	$S(r_T)$	r_T (μm)	$S(r_C)$	r_C (μm)
C1	14.31	0.08	0.05	0.14	0.69	0.08
C2	15.65	0.33	0.08	0.81	0.23	0.66
C3	18.83	1.48	0.06	4.52	0.33	2.26
C4	14.18	0.15	0.06	0.42	0.44	0.22
C5	21.79	0.46	0.12	1.26	0.23	0.81
C6	26.02	0.35	0.08	1.04	0.17	0.66
S7	13.48	2.43	0.15	4.52	0.39	3.02
L8	17.79	28.69	0.09	202.61*	0.67	55.62
L9	16.32	34.18	0.06	202.94*	0.58	51.44
L10	10.80	9.21	0.06	17.79	0.67	13.57
L11	6.36	0.09	0.12	0.18	0.41	0.09
T12	3.51	0.06	0.28	0.30	0.43	0.01
T13	7.31	0.15	0.25	0.61	0.75	0.31
T14	9.00	0.29	0.05	2.20	0.18	0.93
T15	12.34	16.62	0.08	200.00*	0.28	51.44

Figure 3 displays Hölting's classification and the permeability-porosity relationships, which define three tentative permeability groups as a function of the mean pore-throat size, r_M. The boundaries of each permeability field are based on the relationship between water transport coefficient values and the pore size distribution for rocks with open porosity values higher than 10% (or 0.10 expressed as a fraction): (1) upper field: nonvuggy pores visible at first glance with a mean pore-throat radius higher than 1 mm, (2) medium field: a mean pore-throat radius between 1 mm and 0.5 μm, and finally, (3) lower field: a mean pore-throat radius lower than 0.5 μm. Thus, porous rocks with large interparticle pores (pore-throat size higher than 1 mm) and high values of open porosity present high water permeability values. The studied travertine and tufa samples present either separated or touching vugs. Thus, on the one hand, T14 presents

separated vugs that contribute to porosity but not to water permeability, such that the sample has a higher porosity value related to its measured permeability value. This fact can be observed in the difference between the open and total porosities measured in the same sample (Table 1). Large pores of several millimetres in diameter cannot retain water in the saturated-rock weight, and, consequently, they are not quantified in the open porosity calculation. On the other hand, T15 has both separated and touching vugs and therefore has a water permeability value higher than those relative to travertines.

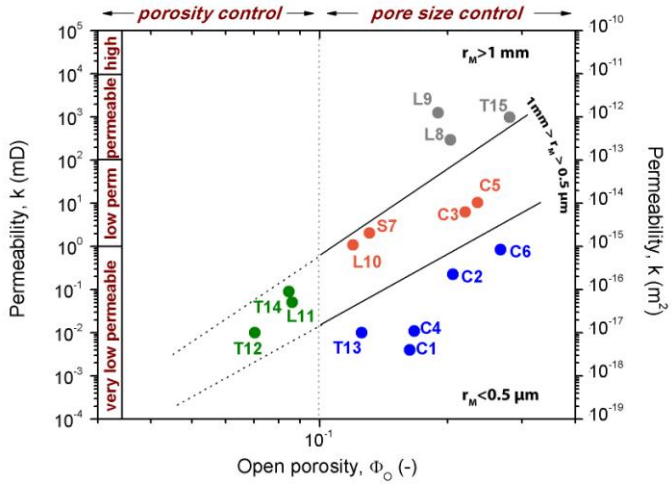

Figure 3. Permeability–porosity relationships of the studied porous building rocks. Permeability divisions correspond to Hölting's classification. Permeability groups: nonvuggy pores visible at first glance and a mean pore-throat radius, r_M, higher than 1 mm; mean pore-throat radius between 1 mm and 0.5 µm; and mean pore-throat radius lower than 0.5 µm.

Pore connectivity is related to a decrease in connected porosity of the coordination number, *z*, of the pore space skeleton.

Figure 3 also includes two zones, in which the transport properties change with porosity. Pore connectivity is related to porosity value. With decreasing porosity, pore chambers and throats evolve differently, and the throats shrink considerably and are eventually destroyed. As a consequence, below 10% connected porosity, pore connectivity dramatically decreases as a

result of the closure and elimination of the throats; meanwhile, in rocks where ϕ > 10%, the reduction of the transport coefficients with porosity is due, almost entirely, to the gradual reduction of the throat dimensions (Wong et al., 1984; Bourbié and Zinszner, 1985; Doyen, 1988; Benavente et al., 2007). Therefore, for porosity values higher than 10%, permeability is related mainly to pore size as described for the proposed permeability fields (r_M > 1 mm; between 1 mm > r_M > 0.5 μm; r_M <0.5 μm). However, for ϕ < 10%, permeability behaviour is influenced by porosity value rather than pore size. Otherwise, T14, L11 and T12 present a mean pore-throat radius of, respectively, 0.29, 0.09 and 0.06 μm (Table 2), and, consequently, they should be placed in the permeability field of r_M < 0.5 μm rather than 0.5 μm < r_M < 1mm.

Figure 4A shows a good relation between water permeability and the water absorption coefficient by capillarity for the majority of the studied rocks. However, the T14 and T15 samples are not well fitted to this relation due to their pore structure. T15 is a tufa and presents well-connected large pores (r > 1 mm), while T14 shows vuggy porosity in the parallel direction of water flow. Both types of pores contribute to increases in the saturated water transport (permeability) but not to the unsaturated flow (capillarity) because capillary forces produced in the interface air-water-pore surface are not sufficient to overcome gravitational forces. As we discuss below, this is supported by Jurin's Law for a wetting liquid, whereby the capillary height for a pore radius of 1 mm is ~1.5 mm, indicating that fluid movement by capillarity would be negligible and that the most important mechanism would be gravitational. Capillary imbibition occurs in pore sizes measuring up to 0.1 μm, although the pore size range between 1 μm and 1 mm promotes high water absorption rates (Benavente, 2011). Large pores provide high water absorption rates for rocks with ϕ > 10% (well-established pore connectivity). This fact sometimes conflicts with conventional thinking in the literature, where the involvement of large pores in capillarity is considered negligible.

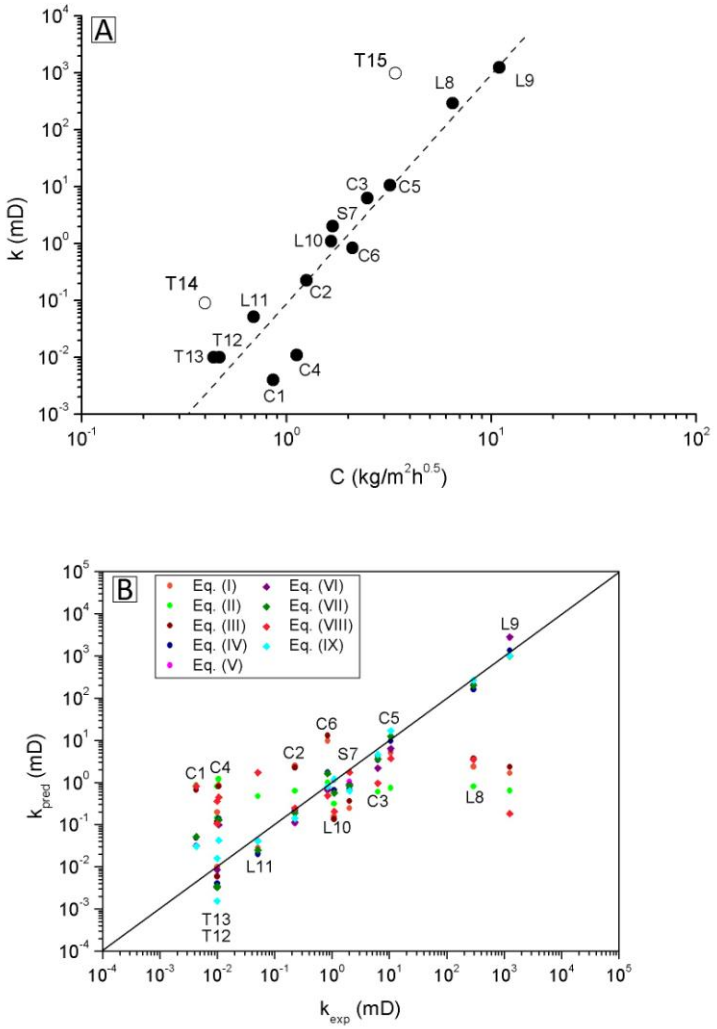

Figure 4. A: Experimental water permeability, k, vs. water absorption coefficient by capillarity, C, in log–log scale. T14 and T15 are not included in the multiple correlations due to the presence of vuggy porosity. B: Comparison of experimental, k_{exp}, and predicted, k_{pred}, water permeability using the linear and multilinear equations in log–log scale. The solid line is the one-to-one correspondence line.

The estimation of water permeability from the pore structure and water absorption coefficient by capillarity is carried out by means of a stepwise multiple regression analysis. Thus, permeability is expressed as a generalized function of several fundamental properties. Variables are logarithmically transformed in order to include more terms and to finally achieve an exponential equation for water permeability. T14 and T15 are not included in the multiple correlations due to the presence of vuggy porosity. Thus, water permeability, k (mD), is taken as a dependent

variable, while open, ϕ_O (%), effective, ϕ_{Hg} (%), and total, ϕ_T (%), porosities, the mean pore radius, r_M (μm) and the water absorption coefficient by capillarity, C ($kg/(m^2 \cdot h^{0.5})$), are considered as independent variables. In the studied rocks, the mean, threshold and critical pore radii present a similar tendency. This means that the Pearson correlation coefficients of the multiple regressions will be alike, although the regression coefficients will be different. We decided to use mean pore radius because it is easy to calculate, it is provided in most of the MIP reports and its calculation does not require the interpretation of the researcher. Table 3 and Figure 4B display the logarithmic and exponential expressions for multilinear regressions.

Eqs. (i)-(iii) represent the classical permeability–porosity relations to characterise flow units in the petroleum industry in terms of open, effective and total porosities. Permeability expressions for each type of porosity value are alike because the porosity values and trends are similar. Some deviations in permeability predictions are found using effective porosity, mainly in rocks with larger pores that MIP cannot measure. This statistical relation is recommended for different samples of similar rocks through a reservoir but not for different types of rocks as we have performed here.

Eq. (iv) and Figure 4B display an interesting relationship between both of the transport coefficients for most of the studied rocks. Eq. (iv) can be expressed in other common units, such as $k\ (mD) = 10^{1.056} \cdot C\ (kg/m^2h^{0.5})^{4.032}$ or $k\ (m^2) = 10^{20.982} \cdot C\ (g/m^2s^{0.5})^{4.032}$.

Eqs. (v) and (vi) include, respectively, open and total porosities to Eq. (iv), and the fitting is slightly increased. In both expressions, the statistical weight of porosity is lower than the capillary coefficient. Eqs. (iv)-(vi) are recommended from a practical point of view because C, ϕ_O and ϕ_T are easy, cheap, Hg-free and can be obtained quickly in the laboratory. Moreover, if the mineralogical composition of the rock is known, the grain density is easily calculated from the mineral density, and, therefore, the total porosity can be calculated without the measurement of the grain density. These procedures are highly recommended for rocks constituted mainly by one mineral (in this situation, the grain density of the rock is equal to the mineral density).

Eqs. (vii) and (viii) contain pore structure parameters obtained from the mercury porosimetry technique (MIP). Eq. (vii) includes the water absorption coefficient by capillarity and mean pore

radius to permeability expression, although fitting is not considerably improved compared to Eqs. (iv)-(vi). C presents more statistical weight in Eq. (vii) than the mean pore radius.

Eq. (viii) presents a poor fit and, therefore, is not recommended for estimating water permeability. In the literature, MIP is successfully used to estimate rock permeability via capillary pressure curves, although it is less used in empirical equations (examples can be found in Schön, 2011).

Finally, the best correlation is found in Eq. (ix), although it is only marginally better than those of Eqs. (iv)-(vi), which do not require MIP. Eq. (ix) incorporates terms for water flow (capillary coefficient) and pore structure (mean throat-pore radius and connected porosity). The capillary coefficient has more statistical weight in Eq. (ix) than the pore structure variables.

Table 3. Logarithmic and exponential expressions linking permeability, k (mD), open, ϕ_O (%), effective, ϕ_{Hg} (%), and total, ϕ_T (%), porosities, mean pore radius, r_M (μm) and capillary absorption coefficient, C ($kg/(m^2 \cdot h^{0.5})$). R is the Pearson correlation coefficient.

Eq.	Logarithmic expression	Exponential expression	R
i	$\log k = -6.373 + 5.157 \log \phi_O$	$k = 10^{-6.373} \cdot \phi_O^{5.157}$	0.5109
ii	$\log k = -1.421 + 1.063 \cdot \log \phi_{Hg}$	$k = 0.04 \cdot \phi_{Hg}^{1.063}$	0.1392
iii	$\log k = -7.208 + 5.808 \cdot \log \phi_T$	$k = 10^{-7.208} \cdot \phi_{Hg}^{5.808}$	0.5714
iv	$\log k = -1.054 + 4.03 \cdot \log C$	$k = 0.09 \cdot C^{4.032}$	0.9527
v	$\log k = 1.265 + 4.587 \cdot \log C - 2.037 \cdot \log \phi_O$	$k = 18.41 \cdot C^{4.587} \cdot \phi_O^{-2.037}$	0.9646
vi	$\text{Log } k = 1.450 + 4.675 \cdot \log C - 2.189 \cdot \log \phi_T$	$k = 28.19 \cdot C^{4.675} \cdot \phi_T^{-2.189}$	0.9645
vii	$\text{Log}k = -1.044 + 3.9779 \log C + 0.084 \log r_M$	$k = 0.09 \cdot C^{3.978} \cdot r_M^{0.084}$	0.9536
viii	$\log k = -0.534 + 0.491 \cdot \log r_M + 0.288 \cdot \log \phi_{Hg}$	$k = 0.29 \cdot r_M^{0.491} \cdot \phi_{Hg}^{0.288}$	0.2853
ix	$\log k = 0.645 + 4.160 \cdot \log C + 0.200 \cdot \log r_M - 1.506 \cdot \log \phi_{Hg}$	$k = 4.42 \cdot C^{4.160} \cdot r_M^{0.200} \cdot \phi_{Hg}^{-1.506}$	0.9700

3.2. Proposed equation: Relationship between capillarity and permeability in rocks with cylindrical pores.

Previous empirical expressions have shown a strong relationship between water permeability and the water absorption coefficient by capillarity and pore structure parameters, including pore radius and porosity. The interpretation of both transport parameters has been carried out via Hagen-Poiseuille's equation. The capillary flow is frequently interpreted by using Washburn's (or Lucas-Washburn's) equation (1921), which consists of applying the Hagen-Poiseuille's equation (1) to the movement of the liquid meniscus in the porous solid. If the gravitational term is negligible, the capillary pressure, Δp, can be written for a straight tube with radius r by the Laplace equation as

$$\Delta p = \frac{2\gamma \cos\theta}{r}, \tag{2}$$

where γ is the interfacial tension and θ is the contact angle. Eq. (2) can be used for porous media if we assume that, locally, a pore can be represented by a tube. Jurin's equation considers that the maximum height, h, that water can rise to is reached when the capillary pressure (Eq. (2)) is equal to the hydrostatic pressure ($\Delta p = \rho g h$, where ρ is the water density and g is the gravitational acceleration). In this situation, the maximum height is equal to $2\gamma\cos\theta/\rho g r$. The rise in the vertical direction, y, is described by Washburn's equation as:

$$y(t) = \sqrt{\frac{r g \cos q}{2h} t} \tag{3}$$

Because the water absorption coefficient by capillarity, C, is obtained from the incremented weight of the water in the rock, Eq. (3) has to be transformed via different steps. First, the rise of one capillary, y, is converted to volumetric uptake in the capillary tube, $dv=\pi r^2 dy$; second, the mass of absorbed water in one pore is calculated from the volumetric uptake by multiplying for water density; and, finally, the weight of one pore is transformed to the weight of the sample via the porosity and normalised by the cross-sectional area of the sample. These transformations consider that the rock is comprised of n parallel capillary tubes, and, therefore, porosity can be written as follows:

$$\phi = \frac{n \cdot \pi \cdot r^2 \cdot L}{S \cdot L} = \frac{n \cdot \pi \cdot r^2}{S}, \quad (4)$$

where S is the macroscopic cross-sectional area of the sample and L is the length of the tube, which is the same as that of the sample. The expression of the weight of absorbed water, W(t), per area can be written as follows,

$$\frac{W(t)}{S} = \phi\rho\sqrt{\frac{r\gamma\cos\theta}{2\eta}t} = C\sqrt{t} \quad (5)$$

where the water absorption coefficient by capillarity, C, is:

$$C = fr\sqrt{\frac{rg\cos q}{2h}}. \quad (6)$$

Detailed derivations of the equations of the water absorption coefficient by capillarity were published in Mosquera et al. (2000); Benavente et al. (2002) and (2007); and Cai et al. (2014). This equation requests a piston-like imbibition process, where the water-air interface is flat. However, this is not always the case in rocks with heterogeneous pore systems (David et al., 2011).

Alternately, Darcy's law empirically describes the fluid flow of a porous rock of cross-sectional area S and length L as follows:

$$q = \frac{k \cdot S}{\eta}\frac{\Delta p}{L}, \quad (7)$$

where k is the permeability. If the capillary tubes are all of the same radius and length, the flow rate q through these bundles of n-tubes can be expressed with Hagen-Poiseuille's equation (1). Equating Eqs. (1) and (7) and inserting Eq. (4) into Eq. (1), Carman-Kozeny's equation is therefore achieved, which expresses permeability as a function of pore size, r, and porosity, ϕ, as follows (Bear, 1988; Dullien, 1992):

$$k = \frac{f \times r^2}{8}. \quad (8)$$

This expression of Carman-Kozeny's equation considers that tortuosity is equal to one and the hydraulic radius equals half the tube radius.

Several authors (Zimmerman and Bodvarsson, 1991; Benavente et al., 2002 and 2007; Scherer, 2004; Espinosa-Marzal and Scherer, 2013) have found that the water absorption coefficient by capillarity (or sorptivity) is proportional to the square root of permeability because Eqs. (6) and (8) are derived from Hagen-Poiseuille's equation for a porous rock constituted by n capillary tubes. Thus, this association can be straightforwardly described by squaring Eq. (6) and inserting Eq. (8), i.e.:

$$C^2 = \phi^2 \rho^2 \frac{r\gamma cos\theta}{2\eta} = \left(\frac{\phi rr}{2 \cdot 4}\right) \frac{4}{r} \frac{\phi \rho^2 \gamma cos\theta}{\eta} = k \frac{4\phi \rho^2 \gamma cos\theta}{\eta r}; \quad (9)$$

Therefore, we propose a simple equation for predicting permeability as follows:

$$k = C^2 \frac{\eta r}{4\phi \rho^2 \gamma cos\theta} \quad (10)$$

Eq. (10) includes information of water fluid rate (water absorption coefficient by capillarity, C), water properties (density, ρ, and viscosity, η), wetting (interfacial tension, γ and contact angle, θ) and pore structure (pore radius, r and porosity, ϕ).

3.3. Goodness of the proposed equation and comparison with various existing models

In Figure 5A, the results obtained with the proposed equation are compared to experimental values, and the influence of the type of pore radius (Table 2) and the wetting are also evaluated. The calculations were carried out using contact angles of 0, 45 and 80º, as we discuss below. Three situations are considered:

(i) k_M: all pores contribute in the same manner to water transport. Therefore, the calculation of Eq. (10) considers the mean pore radius of the entire rock and the effective porosity.

(ii) k_C: water transport is mainly produced through the pore family of larger size. This assumption is based on the fact that larger pores contribute mostly to both water permeability and the water absorption coefficient by capillarity. In rocks with polymodal pore families and well-connected pores, water transfer is easily produced through larger pores rather than small ones. The capillary coefficient quantifies the rate of the weight of absorbed water per unit area; larger pores contribute more to flow rate and weight of absorbed water because they have a

greater volume. Eq. (10) is then calculated using the peak radius, r_C, and the volume fraction of the pore family of larger size (i.e., $\phi_{Hg} \cdot S(r_C)$).

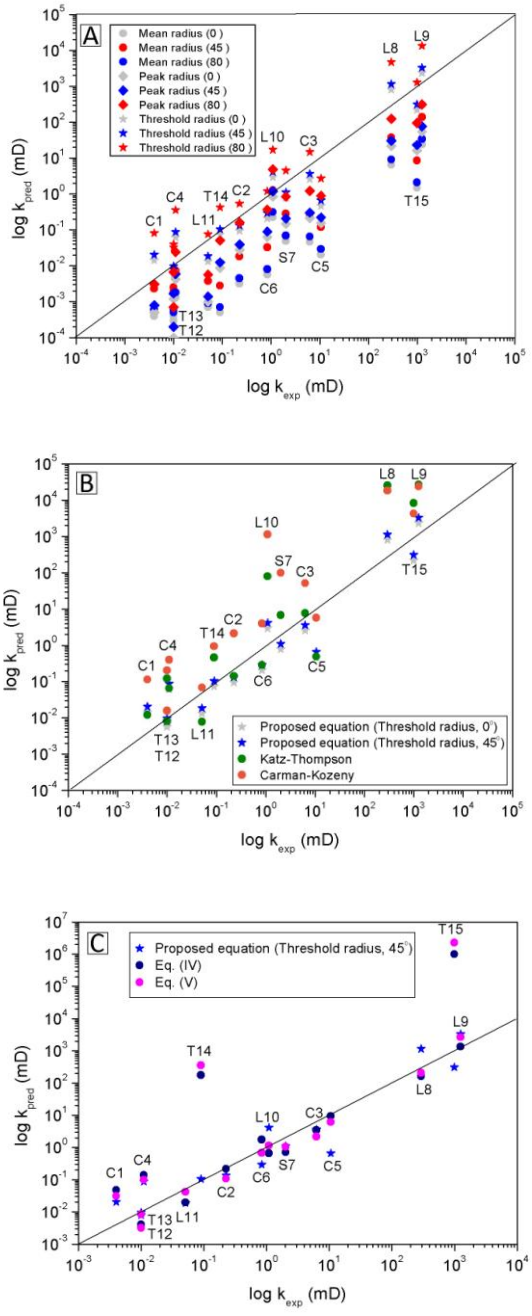

Figure 5. A: Comparison of experimental, k_{exp}, and predicted, k_{pred}, water permeability using the proposed model in log–log scale. Calculations consider contact angles of 0, 45 and 80º and mean, r_M, critical, r_C, and threshold, r_T throat-pore radii. B: Comparison of experimental, k_{exp}, and predicted, k_{pred}, water permeability using the Carman-Kozeny, Katz-Thompson and proposed equations in log–log scale. C: Comparison of experimental, k_{exp}, and predicted, k_{pred}, water permeability using the proposed equation and the empirical equations Eq. (v)-(vi) in log–log scale. The solid line is the one-to-one correspondence line.

(iii) k_T: water flow requires reaching the threshold pore radius to percolate through the rock. Eq. (10) is calculated using the threshold pore radius and the volume of pores larger than the threshold pore radius, (i.e., $\phi_{Hg} \cdot S(r_T)$).

Results show that the best predictions are found for high values of the contact angle and when using the threshold pore radius (k_T). k_M and k_C overestimate experimental permeability, which reflects the importance of the threshold pore radius in the water percolation through the rock.

Wetting is a critical parameter of water transport in unsaturated porous materials. In most of the studies, a total wetting state is considered (the contact angle $\theta = 0^o$). This is certainly true in materials that present a strong affinity for being wetted. Gummerson et al. (1979) reported that, if water absorption is a purely capillarity-driven phenomenon, the sorptivity scales as $(\gamma/\eta)^{1/2}$, where γ is the liquid–air surface tension and η is the viscosity of the liquid. This scaling was found for gypsum plasters, Portland limestones and lime-based composite materials and, subsequently, for many other artificial materials (Hall and Hoff, 2012; and references therein). Numerous studies of sorptivity, however, have called attention to the existence of capillary imbibition anomalies, that is, capillary absorption of water presents a strong deviation of paramount importance from the standard $t^{1/2}$ law. Taylor et al. (2000) noted that the sorptivity value of some limestones was almost 50% lower than the expected for a simple completed wetting capillary scaling. This incomplete wetting was discussed in relation to the natural contamination of the pore surface, which strongly modifies the natural hydrophilic character of calcite by reducing the affinity of its surface for water, inducing a hydrophobic state. They compared sorptivity data obtained from the capillary imbibition of water and a wide range of organic liquids (hydrocarbons and alcohols) carried out at different temperatures in limestones. The results were expressed in terms of the wetting index, β, which indicates a completed wetting condition when $\beta = 1$ and a partial wetting condition when β fluctuates between 0 and 1 ($0 \leq \beta \leq 1$). The later aspect means that there is a finite contact angle controlling the capillary imbibition. Their results confirmed the anomalously low water sorptivity and revealed the existence of water partial wetting. They concluded that the contact angle varies considerably from stone to stone because β lies in the range of 0.11 to 0.72. Sandstones are naturally strongly water-wet in comparison to carbonate rocks. Thus, rocks with a variable ratio of

carbonate-terrigenous minerals (e.g., biocalcarenites) would present a partial wetting. These conclusions can explain why the best outcome of the proposed equation is found for an incomplete wetting state.

Several equations have been developed to correlate pore structure parameters to permeability, such as Carman-Kozeny's (Eq. (8)) and Katz-Thompson's (1986) equations. The Katz-Thompson model uses percolation theory to develop a relationship between air permeability and the threshold pore diameter of sedimentary rocks. Based on the percolation theory, the Katz-Thompson treatment focuses on the steeply rising range of the intrusion curve to identify the first inflection point relating this to the corresponding pressure. Thus, this relationship estimates permeability using data obtained from mercury porosimetry and direct or indirect conductivity measurements (Christensen et al., 1996). Recently, Nishiyama and Yokoyama (2014) applied water-expulsion porosimeter to predict permeability in sedimentary rocks. They obtained interesting results because this technique yields information of transport pores directly serving as flow paths rather than open porosity. The formation factor can be calculated from the optimum and threshold pore radii, the effective porosity and the fractional volume of pores larger than the optimum pore radius (Katz and Thompson, 1987) as follows:

$$k = \frac{1}{56.5} r_T \cdot r_{max}^e \cdot \phi \cdot S(r_{max}^e), \tag{11}$$

where r_{max}^e and r_T are the optimum and threshold pore radii, ϕ is the effective porosity and $S(r_{max}^e)$ is the fractional volume of pores larger than r_{max}^e. The optimum radius is the pore size at which hydraulic conductance is maximum and can be calculated from the procedure described on Katz and Thompson (1987) or by assuming to be equal to $0.34r_T$. As we defined previously, the critical or maximum radius is obtained from the maximum of the pore distribution curve. Table 2 shows a r_C/r_T ratio of 0.25-0.75 for the most of studied rocks, which is in concordance with 0.34 value. Similar values are also found in Nishiyama and Yokoyama (2014). Therefore, we express the Katz-Thompson's equation considering r_{max}^e=0.34·r_T and $S(r_{max}^e) \approx S(r_C)$.

In Figure 5B, (Eq. (8)), Katz-Thompson's equation (Eq. (11)) and the proposed equation (Eq. (10)) are compared to values obtained from experimental results in order to evaluate the applicability of these equations to the studied sedimentary rocks. The Pearson correlation

coefficient between the experimental, k_{exp}, and predicted, k_{pred}, water permeability using the proposed equation, Katz-Thompson's equation and Carman-Kozeny's equation is, respectively, 0.9524, 0.9126 and 0.9184. The results show that the proposed equation obtains the best permeability predictions for the water permeability range of approximately 0.01 mD to 1 D. Katz-Thompson's equation presents better predictions than Carman-Kozeny's equation. In general, both Katz-Thompson's and Carman-Kozeny's equations overestimate the permeability values for the entire permeability, although, in the latter equation, the overestimation is more accentuated (the predicted values are above the one-to-one correspondence line in Figure 5B).

Figure 5C relates the empirical equations (iv)-(vi) and the proposed equation (10). Eqs. (iv)-(vi) include porosities and the water absorption coefficient by capillarity. They present a good fit for permeability and porosity measurements that do not require MIP. However, predictions for T14 and T15 samples are not well due to the presence of vuggy porosity. This was the main reason to exclude them from the multiple correlations in the statistical analysis carried out in section 3.2. The proposed equation (10) is a physics-based approach that includes detailed information about the water absorption coefficient, water properties, wetting and pore structure. Eq. (10) supports the Eqs. (iv)-(vi) and explains the good correlations found using porosities and the water absorption coefficient by capillarity in the prediction of water permeability. Moreover, Eq. (10) yields good predictions for the T14 and T15 samples, such that the proposed model can be recognised as a generalized model for permeability.

As we mentioned previously, L8, L9, and T15 present a volume fraction of pores for $r > 200$ μm that MIP cannot quantify. Therefore, pore structure parameters obtained using MIP become incomplete, and, consequently, permeability estimation throughout the proposed equation (Eq. (10)), Katz-Thompson's equation (Eq. (11)) and Carman-Kozeny's equation (Eq. (8)) should be considered with some reservations. Other limitations also can be found in Eq. (10) for rocks with heterogeneous pore systems, where the imbibition process is not piston-like.

We believe that the proposed equation estimates more realistic water permeability values because it considers parameters involved in the water transport inside of porous rocks. As we discussed previously, both water permeability and capillary imbibition are very sensitive to pore structure, such that any variation in pore structure properties (e.g. by chemical dissolution of

rock, clay swelling, etc.) will be reflected in water transport parameters. Water-rock interaction is therefore influenced and hindered by liquid wetting. Although wettability has typically been studied in the petroleum industry (Dullien, 1992; Schön, 2011), it is less common for construction and building materials. The results show that this parameter should be considered for future research. Conclusions derived from the present study could be extrapolated to other research fields, such as hydrology, soil engineering, unconventional hydrocarbon resources or stone conservation, where water and other fluids move through porous materials.

4. Conclusions

In this paper, water permeability is estimated from capillary imbibition and pore structure for 15 sedimentary rock types. The permeability values range from 10^{-4} to 10^{4} mD ($\sim 10^{-19}$ to 10^{-11} m^2 or $\sim 10^{-12}$ to 10^{-4} m/s). The classical permeability–porosity relationship shows two zones in which the transport properties change with porosity. Below 10% porosity, pore connectivity decreases as a result of the closure and elimination of the throats, and permeability is controlled by porosity values. For porosity values higher than 10%, permeability is related mainly to pore size and describes three permeability-porosity regions in terms of the mean pore-throat radius: 1 mm $< r_M$; between 0.5 μm $< r_M <$ 1 mm; $r_M <$0.5 μm.

The statistical analysis shows a strong relation between water permeability and the pore structure and water absorption coefficient by capillarity. Variables are logarithmically transformed in order to include more terms and to ultimately achieve an exponential equation for water permeability. Nine linear and multiple expressions are fitted, with water permeability expressed as a generalized function of several fundamental properties. The best correlation incorporates terms for water flow (capillary coefficient) and pore structure (mean throat-pore radius and effective porosity). A poor fit is found when using only MIP parameters, such that we do not recommend this expression for estimating water permeability. Empirical equations are finally obtained using open porosity and the water absorption coefficient by capillarity. They present acceptable goodness of fit and are easy, cheap, Hg-free and quickly obtained in the laboratory. Practical aspects are highlighted because water permeability measurement requires more sophisticated procedures than the capillary imbibition test.

We propose a generalized model for permeability that comprises information regarding the water fluid rate (water absorption coefficient by capillarity), water properties (density and viscosity), wetting (interfacial tension and contact angle) and pore structure (pore radius and porosity). Its application is examined in terms of the type of pores that contribute to water transport. The results indicate that the threshold pore radius, in which water percolates through the rock, achieves the best description of the pore system. The analysis of wetting reveals incomplete water wetting in the studied rocks. This questions the widespread use of the complete wetting (the contact angle $\theta = 0^{o}$) in sorptivity and capillary imbibition studies.

The proposed equation is compared against Carman-Kozeny's and Katz-Thompson's equations. The results show that the proposed equation yields the best permeability predictions for the water permeability range of approximately 0.01 mD to 1 D. It considers the parameters involved in the water transport inside porous rocks, such that permeability estimations are realistic in terms of water-rock interactions. However, further research into a wider range of rock types is needed in order to fully apply the proposed equation, particularly where partial wetting is expected, such as in, calcite rocks, sandstones bound by dolomitic cement, dolostones and even lime-based composite materials.

Acknowledgements

This study was financed by the Spanish Ministry of Science and Innovation CGL2011-25162. A pre-doctoral research fellowship was awarded to C. Pla for this project. The authors would also like to express their thanks to C. David and four anonymous reviewers for their comments on an earlier version of this paper.

References

Alam M.M., Fabricius I.L., Prasad M., 2011. Permeability prediction in chalks. Am. Assoc. Pet. Geol. Bull. 95, 1991–2014.

Archie, G.E., 1942. The electrical resistivity log as an aid in determining some reservoir characteristics, Petrol. Trans. AIME 146, 54–62.

Bear J., 1988. Dynamics of Fluids in Porous Media, Elsevier, New York.

Benavente D., Lock P., García-del-Cura M.A, Ordóñez S., 2002. Predicting the capillary imbibition of porous rocks from microstructure. Transp. Porous Media 49, 59–76.

Benavente, D., 2003. Modelización y estimación de la durabilidad de materiales pétreos porosos frente a la cristalización de sales [in Spanish]. PhD Thesis, University of Alicante http://www.cervantesvirtual.com/FichaObra.html?Ref=12011, Accessed: 10/06/2014.

Benavente D., García-del-Cura M.A., Fort R., Ordóñez S., 2004. Durability estimation of porous building stones from pore structure and strength. Eng. Geol. 74, 113–127.

Benavente D., Cueto N., Martínez-Martínez J., García-del-Cura M.A., Cañaveras J.C., 2007. Influence of petrophysical properties on the salt weathering of porous building rocks. Environ. Geol. 52, 197–206.

Benavente D., Cultrone G., Gómez-Heras M., 2008. The combined influence of mineralogy, hydric and thermal properties in the durability of porous building stones. Eur. J. Min. 20, 673–685.

Benavente D., 2011. Why Pore Size Is Important in the Deterioration of Porous Stones Used in the Built Heritage. Macla 15, 41–42.

Bourbie T., Zinszner B., 1985. Hydraulic and acoustic properties as a function of porosity in Fontainebleau sandstone. J. Geophys. Res. 90, 11524–11532.

Brooks R.J., Corey A.T., 1964. Hydraulic properties of porous media. Colorado State University, Colorado.

Cai J., Perfect E., Cheng C.L., Hu X., 2014. Generalized Modeling of Spontaneous Imbibition Based on Hagen−Poiseuille Flow in Tortuous Capillaries with Variably Shaped Apertures. Langmuir. 30, 5142–5151.

Carman P.C., 1937. Fluid flow through a granular bed. Transactions Ins. Chem. Eng. 15, 150–167.

Casteleyn L., Robion P., Collin P.Y., Menéndez B., David C., Desaubliaux G., Fernandes N., Dreux R., Badiner G., Brosse E., Rigollet C., 2010. Interrelations of the petrophysical, sedimentological and microstructural properties of the Oolithe Blanche Formation (Bathonian, saline aquifer of the Paris Basin). Sediment. Geol. 230, 123–138.

Christensen B.J., Mason T.O., Jennings H.M., 1996. Comparison of measured and calculated permeabilities for hardened cement pastes. Cem. Concr. Res. 26,1325–1334.

Choquette P.W., Pray L.C., 1970. Geologic Nomenclature and Classification of Porosity in Sedimentary Carbonates. AAPG Bul. 54, 207- 250.

Cueto N., Benavente D., Martínez-Martínez J., García-del-Cura M.A., 2009. Rock fabric, pore geometry and mineralogy effects on water transport in fractured dolostones, Eng. Geol. 107, 1–15.

David, C., Menéndez, B., Mengus, J.M., 2011. X-ray imaging of water motion during capillary imbibition: Geometry and kinetics of water front in intact and damaged porous rocks, J. Geophys. Res., 116, B03204.

Doyen P.M., 1988. Permeability, conductivity and pore geometry of sandstone. J. Geophys. Res. 93, 7729–7740.

Dullien F.A.L., 1992. Porous Media Fluid Transport and Pore Structure. Academic Press, San Diego.

El-Dieb A.S., Hooton R.D.,1994. Evaluation of the Katz-Thompson model for estimating the water permeability of cement-based materials from mercury intrusion porosimetry data. Cem. Concr. Res. 24, 443–455.

Espinosa-Marzal R.M., Scherer G.W., 2013. Impact of in-pore salt crystallization on transport properties. Environ. Earth Sci. 69, 2657–2669.

Galvañ S., Pla C., Cueto N., Martínez-Martínez J., García-del-Cura MA., Benavente D., 2014. A comparison of experimental methods for measuring water permeability of porous building rocks. Mater. Constr. (in press).

García-del-Cura M.A., Benavente D., Martínez-Martínez J., Cueto N., 2012. Sedimentary structures and physical properties in travertine and carbonate tufa building Stone. Const. Build. Mat. 28, 456–467.

Gummerson R.J., Hall C., Hoff W.D., Hawkes R., Holland G.N., Moore W.S., 1979. Unsaturated water flow within porous materials observed by NMR imaging. Nat. 281, 56–57.

Hall C., Hoff W.D., 2012. Water Transport in Brick, Stone and Concrete. Second ed. Spon Press, London.

Hölting B., 1989. Hydrogeology. An introduction to general and applied hydrogeology. F. Enke Publ., Stuttgart.

Hubbard S.S., Rubin Y., 2000. Hydrogeological parameter estimation using geophysical data: a review of selected techniques. J. Contam. Hydrol. 45, 3–34.

Katz A.J., Thompson A.H., 1986. Quantitative prediction of permeability in porous rock. Phys. Rev. B. 34, 8179–8181.

Katz, A.J., Thompson, A.H. 1987. Prediction of Rock Electrical Conductivity From Mercury Injection Measurements. J Geophys. Res. 92, 599-607.

Kozeny J., 1927. Über kapillare Leitung des Wassers im Boden. Akad. Wiss. Wien, 136, 271–306.

Leverett, M.C., 1940. Capillary behavior in porous solids. Trans. Petrol. AIME 142, 152–169.

Lianbo Z., Xiang-Yang L., 2009. Fractures in sandstone reservoirs with ultra-low permeability: A case study of the Upper Triassic Yanchang Formation in the Ordos Basin, China. Am. Assoc. Pet. Geol. Bull. 93, 461–477.

Lucia F.J., 2007. Carbonate reservoir characterization: an integrated approach. Springer, New York.

Martínez-Martínez J., Benavente D., Gómez-Heras M., Marco-Castaño L., García-del-Cura M., 2013. Non-linear decay of building stones during freeze–thaw weathering processes. Const. Build. Mat. 2, 443–454.

Mosquera M.J., Rivas T., Prieto B., Silva B., 2000. Capillary rise in granitic rocks: interpretation of kinetics on the basis of pore structure. J. Colloid Interf. Sci. 222, 41–45.

Nishiyama N., Yokoyama T., 2014. Estimation of permeability of sedimentary rocks by applying water-expulsion porosimetry to Katz and Thompson model. Eng. Geol. 177, 75-82.

Nokken M.R., Hooton R.D., 2008. Using pore parameters to estimate permeability or conductivity of concrete. Mater. Struct. 41, 1–16.

Panda M.N., Lake, L.W. 1994. Estimation of single-phase permeability from parameters of particle-size distribution. AAPG Bull. 78, 1028-1039.

R Foundation: http://www.r-project.org.

Scherer G.W., 2004. Stress from crystallisation of salt. Cem. Concr. Res. 34, 1613–1624.

Schön J.H., 2011. Physical properties of rocks: fundamentals and principles of petrophysics. Handbook of geophysical exploration, second ed. Elsevier, Oxford.

Taylor, S.C., Hall, C., Hoff, W.D., Wilson, M., 2000. Partial wetting in capillary liquid absorption by limestones. Journal of Colloid and Interface Science, 224, 351-357.

UNE-EN 1936. Natural stone test method. Determination of real density and apparent density, and of total and open porosity. European Committee for Standardization.

Washburn E.W., 1921. The dynamics of capillary flow. Phys. Rev. Lett. 17, 273–283.

Wong P..Z, Koplik J., Tomanic J.P., 1984. Conductivity and permeability of rocks. Phys. Rev. B 30, 6606-6614.

Zimmerman R.W., Bodvarsson G., 1991. A simple approximate solution for horizontal infiltration in a Brooks-Corey medium, Transp. Porous Media 6,195–205.

Highlights

-Permeability expressions are obtained using open porosity and capillary coefficients.

-The permeability – porosity relationship shows two zones defined by a porosity of 10%.

- A generalized model for predicting intrinsic permeability is proposed.

-The analysis of wetting reveals incomplete water wetting in the studied rocks.